Gadolinium-doped iron oxide nanoparticles induced magnetic field hyperthermia combined with radiotherapy increases tumor response by vascular disruption and improved oxygenation

Pei-Shin Jiang[1, 2], Hsin-Yu Tsai[1], Philip Drake[3,] Fu-Nien Wang[1], and Chi-Shiun Chiang[1]

[1] *National Tsing Hua University, Hsinchu, Taiwan*

[2] *Biomedical Technology and Device Research Laboratories, Industrial Technology Research Institute, Hsinchu, Taiwan*

[3] *School of Chemistry and Forensic Sciences, University of Bradford, UK*

Corresponding Author

Chi-Shiun Chiang,

Department of Biomedical Engineering and Environmental Sciences

National Tsing Hua University

101 Sec. 2, Kuang-Fu Rd.

Hsinchu, 30013

Taiwan

Tel: +886 35733168

Fax: +886 35918649

Email: cschiang@mx.nthu.edu.tw

Gadolinium -doped iron oxide nanoparticles induced magnetic field hyperthermia combined with radiotherapy increases tumor response by vascular disruption and improved oxygenation

The gadolinium-doped iron oxide nanoparticles (GdIONP) with greater specific power adsorption rate (SAR) than Fe_3O_4 was developed and its potential application in tumor therapy and particle tracking were demonstrated in transgenic adenocarcinoma of the mouse prostate C1 (TRAMP-C1) tumors. The GdIONPs accumulated in tumor region during the treatment could be clearly tracked and quantified by T2-weighted MR imaging. The therapeutic effects of GdIONP-mediated hyperthermia alone or in combination with radiotherapy were also evaluated. A significant increase in the tumor growth was observed following the treatment of thermotherapy only group (2.5 days), radiation therapy only group (4.5 days), and the combined radio-thermotherapy group (10 days). Immunohistochemical staining revealed a reduced hypoxia region with vascular disruption and extensive tumor necrosis following the combined radio-thermotherapy. These results indicate that GdIONP-mediated hyperthermia can improve the efficacy of radiotherapy by its dual functions in high temperature (temperature greater than 45 degree C)-mediated thermal ablation and mild-temperature hyperthermia (MTH) (temperature between 39 ~ 42 °C)-mediated reoxygenation.

Keywords: nanoparticle; magnetic field hyperthermia; tumor therapy; radiotherapy; thermal ablation

Introduction

Magnetic nanoparticles are widely used for a variety of biomedical application, including targeted delivery of therapeutic agents, hyperthermia treatment of cancers, magnetic resonance (MR) imaging, and biomagnetic separation [1-4]. Magnetic nanoparticles have been suggested as a suitable mediator in conventional thermotherapy for achieving intratumor hyperthermia and reducing side effects [5, 6][7]. Magnetic nanoparticles- mediated thermotherapy involves a coupling of an external magnetic field to heat the tumor areas surrounding the magnetic particles [8-10]. The magnetic particles interact with the magnetic field and dissipate energy to their surroundings, causing a heating effect in deep tissues. The mechanisms that the energy is dissipated are strongly related to the physical and chemical properties of the particles and can be expressed by their specific power adsorption rate (SAR) [11]. We have developed gadolinium-doped iron-oxide nanoparticles (GdIONP) with superparamagnetic characteristics and a higher SAR value than the reported ones of Fe_3O_4 by four times [12, 13]. Radiation therapy has been employed to treat approximately 50% of various cancer patients. The ionizing radiation dosage given to the tumor is determined based on the radiosensitivity of the surrounding normal tissue [14]. Therefore, the tolerant radiation dose is frequently not sufficient to eliminate all loco-regional reoccurrences or cure localized cancers [15]. The success rate of local tumor control by radiation therapy is determined primarily by the number of clonogens [16] and their intrinsic cellular radioresistance, and the microenvironmental factors such as hypoxia. The hypoxia induced by cellular and micro-environmental changes of tumor contribute to tumor aggressiveness and resistance to radiation therapy [15, 17]. Several therapeutic strategies have been developed to overcome the problem of tumor hypoxia [18]. One of the most highly effective therapeutic adjuncts for radiation therapy is mild hyperthermia, which provides both direct anti-tumor [19, 20] as well as the

microenvironment effects [21, 22]. Several preclinical or clinical studies have demonstrated improved responses when tumors were treated with a combination of localized hyperthermia and radiotherapy compared with radiotherapy alone [19, 23] [24]. However, several issues still need to be resolved before hyperthermia can be utilized as a radiation enhancer in routine clinical practices, including a sufficient delivery of thermal doses, the heating duration required, and the problem resulted from the instability of local temperatures. Nanoparticle-induced magnetic field hyperthermia has shown its potential in solving these issues by providing a non-invasive and localized treatment. In the previous studies, we have shown the biocompatibility, thermal profile under alternating magnetic field and superparamagnetic characters of the GdIONP [12, 13]. Herein we further demonstrate the effects of GdIONP-induced magnetic field hyperthermia combined with a radiotherapy and the interaction mechanism in an intramuscular TRAMP-C1 tumor model.

This study demonstrates that the magnetic nanoparticle-mediated hyperthermia caused mixed thermotherapeutic effects such that thermal ablation close to the GdIONP localization while mild hyperthermia at a distant was observed. The results suggest that GdIONP-induced magnetic field hyperthermia enhances the efficacy of radiation therapy by two possible mechanisms: (1) reducing the fraction of hypoxic cells that are resistant to radiation cytotoxic effect and (2) inducing localized tumor-specific vascular disruption and necrosis. This study also presents a simple approach to incorporate the advantages of these two radiation-modifying effects using a single strategy, GdIONP-mediated hyperthermia.

Materials and Methods

Synthesis of Gd-doped iron oxide nanoparticles

Gd-doped iron oxide nanoparticles (GdIONP) were synthesised as described by Drake *et al.* [12]. The detailed synthesis and characterisation can be seen in the supplementary material associated with this paper. The nanoparticle (NPs) composition was $Gd_{0.02}Fe_{2.98}O_4$ as determined by inductive coupled plasma with atomic emission spectroscopy (ICP-AES). The nanoparticle (NPs) composition was $Gd_{0.02}Fe_{2.98}O_4$ as determined by inductive coupled plasma - atomic emission spectroscopy (ICP-AES). The GdIONPs are 13.2 ± 3.1 nm in diameter and superparamagnetic with a magnetisation value (Ms) of 65.67 emu g^{-1}. The magnetisation curve, X-ray diffraction pattern (XRD) and TEM images can be seen in the supplementary material fig S1, S2 and S3 respectively. For use in this study the GdIONPs were given a dextran coating. To achieve this the nanoparticles were dispersed in deionised water and dextran (10000 Mw). After ultrasonic mixing, NH_4OH was added to bring the pH to 10. The mixture was then continuously stirred while being heated to 75 °C and was held at this temperature for 75 min. To remove excess dextran the suspension was dialyzed using a membrane with a molecular weight cut-off (MWCO) at 10000 Daltons. The suspension was then centrifuged at 4000 g for 30 min to remove any large aggregates. Finally, the suspension was filtered through a 0.2 μm filter.

Cells and animals

All experiments were done with the use of 6-to-8-weeks-old male C57BL/6J mice. The transgenic adenocarcinoma of the mouse prostate (TRAMP)-C1 prostate cancer cell line was derived from transgenic mice with adenocarcinoma of the mouse prostate [25] and was purchased from the ATCC (CRL-2730). During the experiments, all mice were cared for in accordance with the guidelines approved by the Institutional Animal Care

and Use Committee (IACUC) of National Tsing Hua University, Taiwan (approved number: IACUC:09705). Tumors were generated by intramuscular injection (i.m.) of $3*10^6$ viable cells into the thigh. Mice with tumors with 4 to 6 mm in diameter were selected and randomly allocated to groups for experimentation (tumor diameter was defined as the diameter of tumor-bearing leg – the diameter of control mouse leg, in which the diameter is defined as ((the length of long axis at the tumor region + the length of short axis at the tumor region)/2), and the tumor volume in mm^3 was calculated by the formula: volume = 4/3 x 3.1416 x $(diameter/2)^3$, in which at least 5 mice were evaluated at each time point.

Radiotherapy and Thermotherapy

The mice were randomly divided into four groups for the different treatments: (1) no treatment as control, (2) a single dose radiation therapy (RT) of 25 Gy, (3) twice of the 40-min GdIONP-mediated thermotherapy (TT) using magnetic field hyperthermia (500 Ampere and 200 Gauss) separated by 16-hour interval, (4) a combined treatment (RT + TT) using a 25 Gy radiation therapy followed by a thermotherapy (radio-thermotherapy) 30 minutes afterward (see supplement Fig. S4). The mice in TT and RT+TT group were injected with 0.05ml GdIONP in saline before the magnetic field hyperthermia, and the mice in control and RT groups were injected with 0.05ml saline without hyperthermia treatment. This combined therapeutic protocol was designed according to the suggested best combined sequence [14]. Mice were anesthetized by a mixture of ketamine and xylazine and restrained by adhesive tape during irradiation, thermotherapy, and MRI imaging. A single dose irradiation of 25 Gy was delivered to the tumor site using 6 MV X-rays from a linear accelerator with a dose rate of 2.3 Gy/min and a 1.5 cm bolus on the surface, with the rest of body shielded. GdIONP (1 mg) prepared in 0.05 mL saline was intratumorally injected into the tumors. The groups receiving TT were then

subjected to an induction heating operated at 52 kHz and 246 Oe. The tumor size was then monitored by daily recording the diameter measured by Vernier calliper. For mice receiving two injections of either nanoparticles or saline solutions for the blank control group, the 1st injection were conducted at the start of treatment or after RT, and the 2nd injection were carried out 16 hours after the 1st injection. The temperature read by the thermocouple needle positioned at the tumor core (or injection site) was continuously recorded during the magnetic hyperthermia. The effect of comparison among groups was made with tumor growth delay that was defined as the time taken for a treated tumor to grow to 350 cubic mm after treatment and compared with control.

Immunohistochemistry and image analysis

For detecting hypoxia, pimonidazole hydrochloride (Hypoxyprobe-1 Kit; Chemicon) was administered as 4 mg in 0.1 mL by intravenous injection (i.v.). One hour after administration of the hypoxia reagent [26], the tumors were removed and stored in optimal cutting temperature compounds at -80 degree C. For immunohistochemical staining, ten-micrometer cryostat sections were fixed in methanol at -20 degree C for 10 min and then rehydrated in PBS. Nonspecific binding was blocked by incubating the sections in 1% bovine serum albumin in PBS for 30 min. Tumor sections were double stained for pimonidazole (PIMO) and CD31. Pimonidazole was detected with the mouse antibody (Chemicon) and goat anti-mouse IgGγ1 Alexa 488 (Invitrogen). For labelling endothelial cells, rat anti-CD31 antibody (BD Biosciences) and then a secondary goat anti-rat antibody conjugated with Alexa 594 (Invitrogen) was utilized. Slides were rinsed in PBS and mounted with ProLong Gold antifade reagent with DAPI (P-36931; Invitrogen). Sections stained by standard H&E reagent (Merck) were used to identify the necrotic areas.

Immunofluorescent images from each tumor section were captured with the use

of an external digital camera (DXM-1200C; Nikon) on a Nikon fluorescence microscope (Nikon Eclipse TE 2000-S). Scanning at X100 magnification yielded composite images of endothelial cells with the perfusion marker and pimonidazole. Composite images were obtained at X200 or X630 magnification. The images were analyzed by Image-Pro version 4 software (Media Cybernetics). Microvascular density (MVD) was determined as the number of pixels positive for CD31 divided by the total tumor area. Regions of gross necrosis were visually identified on the H&E images and were outlined with a multiple-area-of-interest tool to determine the percentage in total tumor area. The hypoxia fraction was defined as the area positive for pimonidazole divided by the total tumor area (necrosis excluded). Data are presented as means with standard deviation. Statistical analyses used GraphPad Prism version 3 (GraphPad Software). For all comparisons, assessment of statistical significance was by unpaired t tests or one-way ANOVA with significance set at $P \leqq 0.05$.

MR imaging

All magnetic resonance imaging (MRI) scans were acquired on a 7-T animal MRI scanner (Bruker ClinScan 70/30). The imaging parameters for the T1-weighted images of pre-GdIONP injection were as follows: repetition time (TR) / echo-time (TE) / Flip angle = 600 ms/ 3.81 ms/ 25 degree, slice thickness = 0.5 mm, matrix size = 176 X 256 and field-of-view (FOV) = 27 X 40 mm. 1 mg GdIONPs in 0.05 mL of saline were intratumorally injected. The T1-weighted imaging parameters were used: TR/ TE/ Flip angle = 600 ms/ 3.81 ms/ 25 degree, slice thickness = 0.5 mm, matrix size = 176X 256 and FOV = 34 X 50 mm. T2-weighted images were then acquired to confirm no anatomical change after GdIONPs injection. The following parameters were used: TR/ TE/ Flip angle = 3140 ms/ 38 ms/ 180 degree, slice thickness = 1 mm, matrix size = 228 X 320, FOV = 25 X 35 mm.

Results

Combined GdIONPs-mediated hyperthermia with radiation therapy enhances tumor growth delay

In order to assess the influences of GdIONPs-mediated hyperthermia on radiation therapy-induced tumor growth delay, the tumor size of individual mouse in each treatment group was measured daily by calliper (Figure 1). The tumor growth curve shows that the radiotherapy (RT) and thermotherapy (TT) had similar effect on tumor growth delay (2.5 and 4.5 days, respectively), while tumor growth were delayed more than 10 days by the combined therapy (RT+TT). This result suggests that the GdIONPs-mediated hyperthermia could significantly increase the efficacy of radiation therapy for TRAMP-C1 tumor.

GdIONP mediated hyperthermia

The distribution of the injected GdIONPs was investigated using T1 and T2 MRI as shown in Figure 2A. Images showed that the injected GdIONPs remained concentrate in TRAMP-C1 tumors after the hyperthermia treatment for 10, 30, and 50 minutes. The temperature profile (Figure 2B) recorded by thermocouple needle showed that the temperature of at the cord of tumor tissue exceeded 45 degree C after hyperthermia treatment for more than 40 minutes. The simulated temperature distribution profile (Figure 2C) [27] showed that the tumor temperature decreases 1.5 degree C for each 2 mm. This indicates that GdIONP-mediated thermal effect may not be the same at the different regions, which depends on the distance to the injection site.

Anti-tumor and microenvironmental effects

Hematoxylin and Eosin (H&E) and PIMO staining were used to examine the pattern of necrosis and hypoxia, respectively, of tissues at day 1 and week 1 post GdIONP-induced thermotherapy, and the necrotic regions were highlighted by the yellow outlines in Figure 3. While there is no regular necrotic pattern in control tumors at day 1, the necrotic regions in thermotherapy-treated tissue were mainly located in the areas with intensive signal of T2 image (Fig 2A). This is in consistent with our previous report that the necrotic region induced by TT was co-localized with GdIONP deposition from the analysis obtained by the laser ablation/inductively coupled plasma (LA-ICP-MS) mapping technique [28]. PIMO staining revealed large continuous hypoxia zones surrounding the necrotic regions. When the areas of the necrotic and hypoxic regions were calculated (Fig. 3E and 3F), it appeared that the ratios of necrosis and hypoxia in the control tumors were increased as the tumors grew. However, the necrotic region was significantly increased one day after TT, and the ratio was maintained high for one week after treatment. It is worth noting that the ratio of hypoxia was not increased with the increase of necrotic region at week one after TT as observed in the control group. This supports the hypothesis that two working mechanisms were involved in the GdIONP-mediated hyperthermia therapy. In order to better characterize the effect of these two working mechanisms, the tissues were counterstained by PIMO for hypoxia and CD31 for vessels (Fig. 4A). The CD31 positive cells of the control group were randomly distributed all over the tumor, suggesting the vessels were intervened throughout the hypoxia and necrosis regions (Fig. 4A). This is consistent with a general opinion that the hypoxia and necrosis of growing tumors mainly due to the malfunction of tumor vessels [26].

In contract, almost no vessels were observed in the necrotic regions at day 1 post TT. The microvascular density (MVD) in the non-necrotic regions (Fig. 4B) did not

significantly change at day one and week one post TT. This again supports the theory that thermal ablation effect took place at regions subject to high temperature and resulted in massive vessel disruption and necrosis, while the MTH on the contrary did not cause significant impact on vessel numbers. We further evaluated the changes in necrosis, hypoxia, and MVD of the tumor specimens for the four experimental groups, (control, RT, TT, and RT+TT), at 15 days post treatment despite that the control tumor was removed at day 10 due to ethical issue (Fig. 5A). As the inference from the previous experiments, the necrosis ratio in tumor of the control group was further increased to 44.3% (Fig.5B) while the ratio of hypoxia was maintained at a 15.4% level (Fig. 5C). This might be owing to the relative constant MVD at untreated tumors (Fig. 5D). It should be noted that the necrotic region was excluded from the calculation of hypoxia ratio and MVD.

On the other hand, although the 25 Gy of irradiation (RT group) and the two-dose 40-min GdIONP-mediated thermotherapy (TT group) produced similar tumor growth delay (Fig. 1), they might contribute differently to the changes of necrosis, hypoxia, and MVD. The tissues from TT-treated tumors had a higher percentage of necrosis, lower percentage of hypoxia, and higher MVD than those in RT-treated tissues. This indicates different anti-tumor mechanisms might be involved in RT versus TT. The combined radio-thermotherapy had the greatest effect on reducing tumor size and brought about higher percentage of necrosis (21.87%, Fig. 5B) and hypoxia (~13%, Fig.5C), but mixed results in MVD (Fig. 5D). This indicates a complex interactive mechanism between RT and TT.

Discussion

This study describes the anti-tumor effect and microenvironmental changes after the

GdIONP mediated thermotherapy, radiation therapy or combined radio-thermotherapy. The results suggest that the combined radio-thermotherapy can significantly inhibit tumor growth better than RT or TT alone. The enhancement of radiation therapy by GdIONP-mediated thermotherapy resulted from a mixed thermotherapeutic effect, high temperature-mediated thermal ablation and mild-temperature hyperthermia (MTH)-mediated tumor reoxygenation. It has been shown that thermal ablation could lead to tumor destruction by direct cell necrosis, coagulation, and protein denaturation [29]. The significant increase of necrosis percentage one day after TT and the spatial correlation of necrosis pattern and GdIONP distribution tracked by MR imaging support the ablation effect of the GdIONP induced hyperthermia (Temperature >45degrees C). The dysfunction of the vessel collapsed at GdIONP-concentrated regions was due to the thermo-sensitive response of vessels in tumors. The tumor vasculature system is less capable in heat dissipation owing to blood flow reduction and therefore is more likely to be damaged by hyperthermia [30-32]. Owing to inefficient blood flow and oxygen transported by the immature blood vessels the tumor cells reside in an acidic and nutrient-deprived environment that confers them greater thermosensitivity. This is the main effect contributed by high temperature TT. The effect of TT on vessel networks was not so evident when the MVD of non-necrotic area only was used for evaluation. However, decrease in the number of vessels and enlargement in vessel diameter were observed. It has been suggested that blood flow and perfusion could be increased by mild hyperthermia (heating to 39 – 42℃) [14, 31, 33]. Due to the temperature gradients induced by the magnetic nanoparticle in hyperthermia (Fig. 2C), a mild hyperthermia effects could occur on the periphery of the GdIONP concentrated region. The temperature gradient of tumor is - 0.75 degree C/mm from the centre of MNPs for multi-layer structures such as skin, fat and muscle according to the numerical analysis

results of MNPs mediated hyperthermia [27]. MR imaging and laser ablation/inductively coupled plasma (LA-ICP-MS) mapping showed that GdIONP were localized in the injected site throughout the hyperthermia and remained within an area of 3 to 5 mm in diameter inside the tumor for two weeks after TT [28]. The temperature at tumor core was more than 45 degree C and decreased from 43 degree C to 40 degree C at 2.7 mm to 6.7 mm away from the GdIONPs-deposited region (Fig. 2C). Therefore, the periphery of GdIONP concentrated-tumor core might be subject to mild-hyperthermia. This is possibly the reason that the hypoxia ratio in the TT-treated group was the lowest among all four groups after two weeks (Fig. 5C). It needs to remind that the TT was given on day 0. The histological data that we saw from the samples of week 2 were a re-growing tumor, of which the microenvironment was affected by the tumor microenvironment altered by the TT therapy at day 0. In opposite to the thermotherapy, RT resulted in small and dispersed necrosis areas [26]. The combined radio-thermotherapy produced both effects thus resulting in large necrotic areas in GdIONP-concentrated tumor core and small necrosis in the surroundings. This partially explains the increased effect on the tumor growth delay (Fig. 1). It also indicated that GdIONP-mediated hyperthermia and RT might have complementary role in tumor therapy. In addition to the reduction in MVD, RT, as TT, it also resulted in increase in vessel diameter, which is in consistent with the published results [26, 34]. These results demonstrate that TT and RT not only have complementary anti-tumor effect, but also result in vessel dilation.

In this study, the TT was applied after RT since it has been reported that such schedule yielded the best enhancement for RT through heat [23]. Hyperthermia acts as a potent and selective radiosensitizer by three major possible mechanisms: (1) inhibiting or impairing DNA repair, (2) devastating the radioresistant and hypoxic tumor cells, (3)

altering the vascular microenvironment [14]. The combination of heat and radiation in a clinical regimen will probably be conducted in a fractionated schedule. For clinical practice a pronounced treatment could be realised by adjusting the sequence, frequency, dosage, duration and the intermittent time for conjointly administering the two modalities [35-37]. The combined radio-thermotherapy protocol used in this study contributed to the reduction in hypoxia and generated similar vascular patterns as the RT alone, indicating the involvement of mild hyperthermia effect implied by the observed enhanced effects from the tumor growth curve.

Conclusion

The GdIONP in this study were demonstrated to have a high SAR value and superparamagnetic characteristic [15]. The improved SAR value of this Gd-doped system can be translated into improved tumor therapy [16]. The MR imaging and LA-ICP-MS mapping verified the stability of the nanoparticles with no decomposition evident in the tissue and their potential usage as T2 contrast agents [30]. In this study, we further demonstrate that GdIONP-mediated thermotherapy delivered mixed thermotherapeutic effects, showing thermal ablation in Gd-IONP deposited region and mild hyperthermia away from the thermal ablation region. The approach enhances the efficacy of radiation therapy by reducing the fraction of hypoxic cells that contribute to radiation resistance and by inducing tumor-specific localized vascular disruption and necrosis. This study also presents a simple means to combine the advantages of these two radiation-modifying effects using a single strategy, GdIONP-mediated hyperthermia. The multiple modalities of the GdIONP highlight the potential for biomedical application.

Declaration of interest

The author reports no conflicts of interest. The author alone is responsible for the content and writing of the paper.

Acknowledgment

This work is supported by MOST 104-2627-M-007-008 from the Ministry of Science and Technology, 104N2741E1 from National Tsing Hua University, and 104-EC-17-A-22-0777 from Ministry of Economic Affairs, Taiwan.

References

1. Hiergeist R, Andra W, Buske N, Hergt R, Hilger I, Richter U, et al. Application of magnetite ferrofluids for hyperthermia. Journal of Magnetism and Magnetic Materials. 1999;201:420-2. doi: 10.1016/s0304-8853(99)00145-6. PubMed PMID: WOS:000081120800110.
2. Pankhurst QA, Connolly J, Jones SK, Dobson J. Applications of magnetic nanoparticles in biomedicine. Journal of Physics D-Applied Physics. 2003;36(13):R167-R81. doi: 10.1088/0022-3727/36/13/201. PubMed PMID: WOS:000185360900004.
3. Duguet E, Vasseur S, Mornet S, Devoisselle J-M. Magnetic nanoparticles and their applications in medicine. Nanomedicine. 2006;1(2):157-68. doi: 10.2217/17435889.1.2.157. PubMed PMID: WOS:000243835000006.
4. Yallapu MM, Othman SF, Curtis ET, Gupta BK, Jaggi M, Chauhan SC. Multi-functional magnetic nanoparticles for magnetic resonance imaging and cancer therapy. Biomaterials. 2011;32(7):1890-905. doi: 10.1016/j.biomaterials.2010.11.028. PubMed PMID: WOS:000287069400015.
5. Jordan A, Scholz R, Wust P, Fahling H, Felix R. Magnetic fluid hyperthermia (MFH): Cancer treatment with AC magnetic field induced excitation of biocompatible superparamagnetic nanoparticles. Journal of Magnetism and Magnetic Materials. 1999;201:413-9. doi: 10.1016/s0304-8853(99)00088-8. PubMed PMID: WOS:000081120800109.
6. Moroz P, Jones SK, Gray BN. Magnetically mediated hyperthermia: current status and future directions. International Journal of Hyperthermia. 2002;18(4):267-84. doi: 10.1080/02656730110108785. PubMed PMID: WOS:000176300100001.
7. Salunkhe AB, Khot VM, Pawar SH. Magnetic hyperthermia with magnetic nanoparticles: a status review. Curr Top Med Chem. 2014;14(5):572-94. PubMed PMID: 24444167.

8. Rosensweig RE. Heating magnetic fluid with alternating magnetic field. Journal of Magnetism and Magnetic Materials. 2002;252(1-3):370-4. doi: 10.1016/s0304-8853(02)00706-0. PubMed PMID: WOS:000179686200116.
9. Babincova M, Altanerova V, Altaner C, Cicmanec P, Babinec P. In vivo heating of magnetic nanoparticles in alternating magnetic field. Medical Physics. 2004;31(8):2219-21. doi: 10.1118/1.1767101. PubMed PMID: WOS:000223316600006.
10. Wang XM, Gu HC, Yang ZQ. The heating effect of magnetic fluids in an alternating magnetic field. Journal of Magnetism and Magnetic Materials. 2005;293(1):334-40. doi: 10.1016/j.jmmm.2005.02.028. PubMed PMID: WOS:000229661400052.
11. Ma M, Wu Y, Zhou H, Sun YK, Zhang Y, Gu N. Size dependence of specific power absorption of Fe3O4 particles in AC magnetic field. Journal of Magnetism and Magnetic Materials. 2004;268(1-2):33-9. doi: 10.1016/s0304-8853(03)00426-8. PubMed PMID: WOS:000186714900006.
12. Drake P, Cho H-J, Shih P-S, Kao C-H, Lee K-F, Kuo C-H, et al. Gd-doped iron-oxide nanoparticles for tumor therapy via magnetic field hyperthermia. Journal of Materials Chemistry. 2007;17(46):4914-8. doi: 10.1039/b711962c. PubMed PMID: WOS:000251269300013.
13. Jiang P-S, Drake P, Cho H-J, Kao C-H, Lee K-F, Kuo C-H, et al. Tailored Nanoparticles for Tumor Therapy. Journal of Nanoscience and Nanotechnology. 2012;12(6):5076-81. doi: 10.1166/jnn.2012.4890. PubMed PMID: WOS:000306861000098.
14. Horsman MR, Overgaard J. Hyperthermia: a potent enhancer of radiotherapy. Clinical Oncology. 2007;19(6):418-26. doi: 10.1016/j.clon.2007.03.015. PubMed PMID: WOS:000248780400005.
15. Moeller BJ, Richardson RA, Dewhirst MW. Hypoxia and radiotherapy: opportunities for improved outcomes in cancer treatment. Cancer and Metastasis Reviews. 2007;26(2):241-8. doi: 10.1007/s10555-007-9056-0. PubMed PMID: WOS:000248300100003.
16. Tarnawski R, Kummermehr J, Trott KR. The radiosensitivity of recurrent clones of an irradiated murine squamous cell carcinoma in the in vitro megacolony system. Radiotherapy and Oncology. 1998;46(2):209-14. doi: 10.1016/s0167-8140(97)00165-5. PubMed PMID: WOS:000072271600012.
17. Zhang Y, Li M, Yao Q, Chen C. Recent advances in tumor hypoxia: Tumor progression, molecular mechanisms, and therapeutic implications. Medical Science Monitor. 2007;13(10):RA175-RA80. PubMed PMID: WOS:000250332000019.
18. Iversen AB, Busk M, Horsman MR. Induction of hypoxia by vascular disrupting agents and the significance for their combination with radiation therapy. Acta Oncol. 2013;52(7):1320-6. doi: 10.3109/0284186X.2013.825050. PubMed PMID: 23988183.
19. Kampinga HH, Dikomey E. Hyperthermic radiosensitization: mode of action and clinical relevance. International Journal of Radiation Biology. 2001;77(4):399-408. PubMed PMID: WOS:000167998200001.
20. Wust P, Hildebrandt B, Sreenivasa G, Rau B, Gellermann J, Riess H, et al. Hyperthermia in combined treatment of cancer. Lancet Oncology. 2002;3(8):487-97. doi: 10.1016/s1470-2045(02)00818-5. PubMed PMID: WOS:000177436300021.
21. Diagaradjane P, Shetty A, Wang JC, Elliott AM, Schwartz J, Shentu S, et al. Modulation of in vivo tumor radiation response via gold nanoshell-mediated vascular-focused hyperthermia: Characterizing an integrated antihypoxic and localized vascular

disrupting targeting strategy. Nano Letters. 2008;8(5):1492-500. doi: 10.1021/nl080496z. PubMed PMID: WOS:000255906400040.
22. Griffin RJ, Dings RPM, Jamshidi-Parsian A, Song CW. Mild temperature hyperthermia and radiation therapy: Role of tumor vascular thermotolerance and relevant physiological factors. International Journal of Hyperthermia. 2010;26(3):256-63. doi: 10.3109/02656730903453546. PubMed PMID: WOS:000276623900006.
23. Johannsen M, Thiesen B, Gneveckow U, Taymoorian K, Waldofner N, Scholz R, et al. Thermotherapy using magnetic nanoparticles combined with external radiation in an orthotopic rat model of prostate cancer. Prostate. 2006;66(1):97-104. doi: 10.1002/pros.20324. PubMed PMID: WOS:000234121400010.
24. Attaluri A, Kandala SK, Wabler M, Zhou H, Cornejo C, Armour M, et al. Magnetic nanoparticle hyperthermia enhances radiation therapy: A study in mouse models of human prostate cancer. Int J Hyperthermia. 2015;31(4):359-74. doi: 10.3109/02656736.2015.1005178. PubMed PMID: 25811736; PubMed Central PMCID: PMCPMC4696027.
25. Foster BA GJ, Kwon ED, Madias C, Greenberg NM. Characterization of prostatic epithelial cell lines derived from transgenic adenocarcinoma of the mouse prostate (TRAMP) model. Cancer Res. 1997;57:5.
26. Chen F-H, Chiang C-S, Wang C-C, Tsai C-S, Jung S-M, Lee C-C, et al. Radiotherapy Decreases Vascular Density and Causes Hypoxia with Macrophage Aggregation in TRAMP-C1 Prostate Tumors. Clinical Cancer Research. 2009;15(5):1721-9. doi: 10.1158/1078-0432.ccr-08-1471. PubMed PMID: WOS:000263851900025.
27. Wang Q, Deng ZS, Liu J. Theoretical evaluations of magnetic nanoparticle-enhanced heating on tumor embedded with large blood vessels during hyperthermia. Journal of Nanoparticle Research. 2012;14(7). doi: 10.1007/s11051-012-0974-6. PubMed PMID: WOS:000306058900032.
28. Hsieh Y-K, Jiang P-S, Yang B-S, Sun T-Y, Peng H-H, Wang C-F. Using laser ablation/inductively coupled plasma mass spectrometry to bioimage multiple elements in mouse tumors after hyperthermia. Analytical and Bioanalytical Chemistry. 2011;401(3):909-15. doi: 10.1007/s00216-011-5144-7. PubMed PMID: WOS:000292970200016.
29. Diederich CJ. Thermal ablation and high-temperature thermal therapy: Overview of technology and clinical implementation. International Journal of Hyperthermia. 2005;21(8):745-53. doi: 10.1080/02656730500271692. PubMed PMID: WOS:000233906600011.
30. Song CW. Effect of Local Hyperthermia on Blood Flow and Microenvironment: A Review. Cancer Res. 1984;44:10.
31. Song CW, Shakil A, Osborn JL, Iwata K. Tumor oxygenation is increased by hyperthermia at mild temperatures. International Journal of Hyperthermia. 2009;25(2):91-5. doi: 10.1080/02656730902744171. PubMed PMID: WOS:000264750400001.
32. Hokland SL, Nielsen T, Busk M, Horsman MR. Imaging tumor physiology and vasculature to predict and assess response to heat. International Journal of Hyperthermia. 2010;26(3):264-72. doi: 10.3109/02656730903585982. PubMed PMID: WOS:000276623900007.
33. Song CW, Park HJ, Lee CK, Griffin R. Implications of increased tumor blood flow and oxygenation caused by mild temperature hyperthermia in tumor treatment. International Journal of Hyperthermia. 2005;21(8):761-7. doi: 10.1080/02656730500204487. PubMed PMID: WOS:000233906600013.

34. Jain RK. Normalization of tumor vasculature: An emerging concept in antiangiogenic therapy. Science. 2005;307(5706):58-62. doi: 10.1126/science.1104819. PubMed PMID: WOS:000226214300031.
35. Johannsen M, Jordan A, Scholz R, Koch M, Lein M, Deger S, et al. Evaluation of magnetic fluid hyperthermia in a standard rat model of prostate cancer. Journal of Endourology. 2004;18(5):495-500. doi: 10.1089/0892779041271715. PubMed PMID: WOS:000222478400032.
36. Johannsen M, Gneveckow U, Eckelt L, Feussner A, Waldofner N, Scholz R, et al. Clinical hyperthermia of prostate cancer using magnetic nanoparticles: Presentation of a new interstitial technique. International Journal of Hyperthermia. 2005;21(7):637-47. doi: 10.1080/02656730500158360. PubMed PMID: WOS:000233115300004.
37. Johannsen M, Gneueckow U, Thiesen B, Taymoorian K, Cho CH, Waldofner N, et al. Thermotherapy of prostate cancer using magnetic nanoparticles: Feasibility, imaging, and three-dimensional temperature distribution. European Urology. 2007;52(6):1653-62. doi: 10.1016/j.eururo.2006.11.023. PubMed PMID: WOS:000251409600019.

Figures and Table

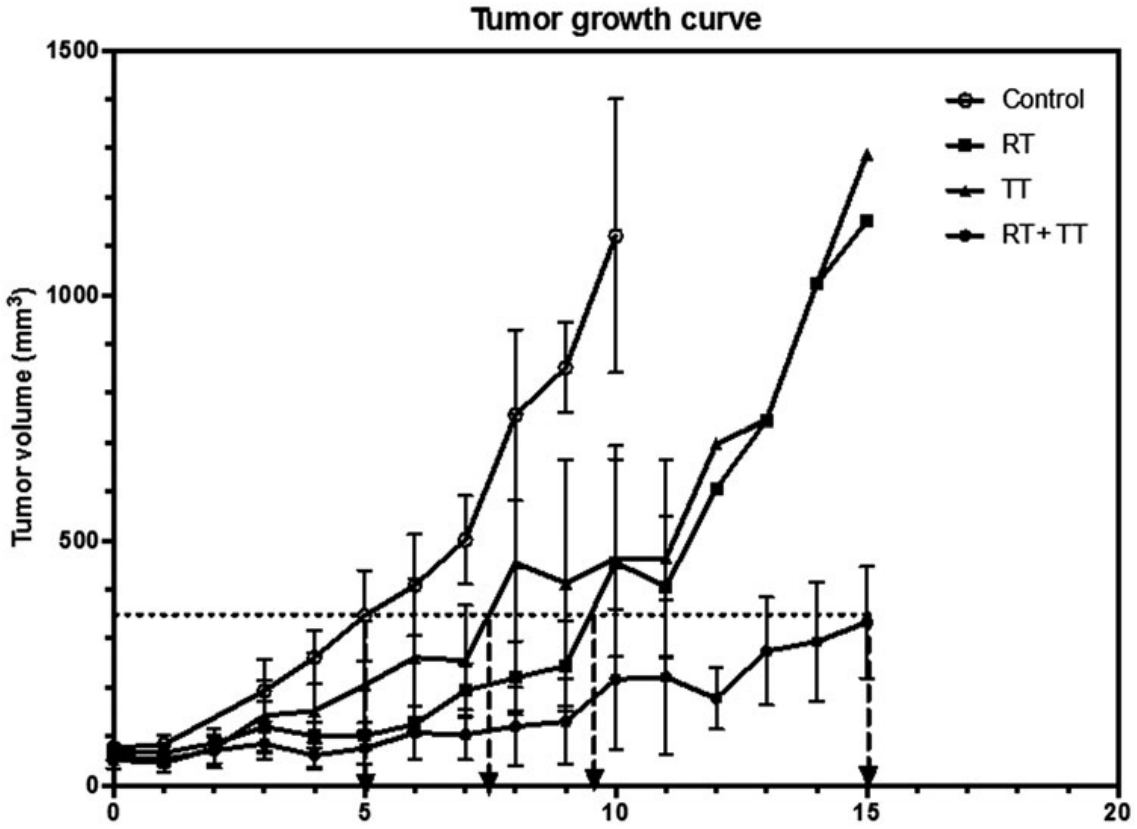

Fig. 1 Tumor growth curves after various treatments. Combined therapy (RT+TT) has resulted in longer tumor growth delay (~10 days) than the radiotherapy (RT, ~4.5 days) or the GdIONP mediated thermotherapy (TT, ~2.5 days) only. TRAMP-C1 cells (1×10^6) were injected intramuscularly into the tights of male C57BL/6J mice. Mice with a palpable tumor of approximately 60 mm^3 in volume were randomly separated into four groups (n=5) and were given 2 times intratumor injections of GdIONP or saline before thermotherapy. Mice were anesthetized before treatments. For the control and RT group, 0.05 ml saline alone was injected. For TT and RT+TT group, 1 mg GdIONP prepared in 0.05 ml saline was injected. TT group were subjected to induction heating at 52 kHz and 246 Oe. In the end of each experiment, mice were sacrificed and the tumors were excised and weighed.

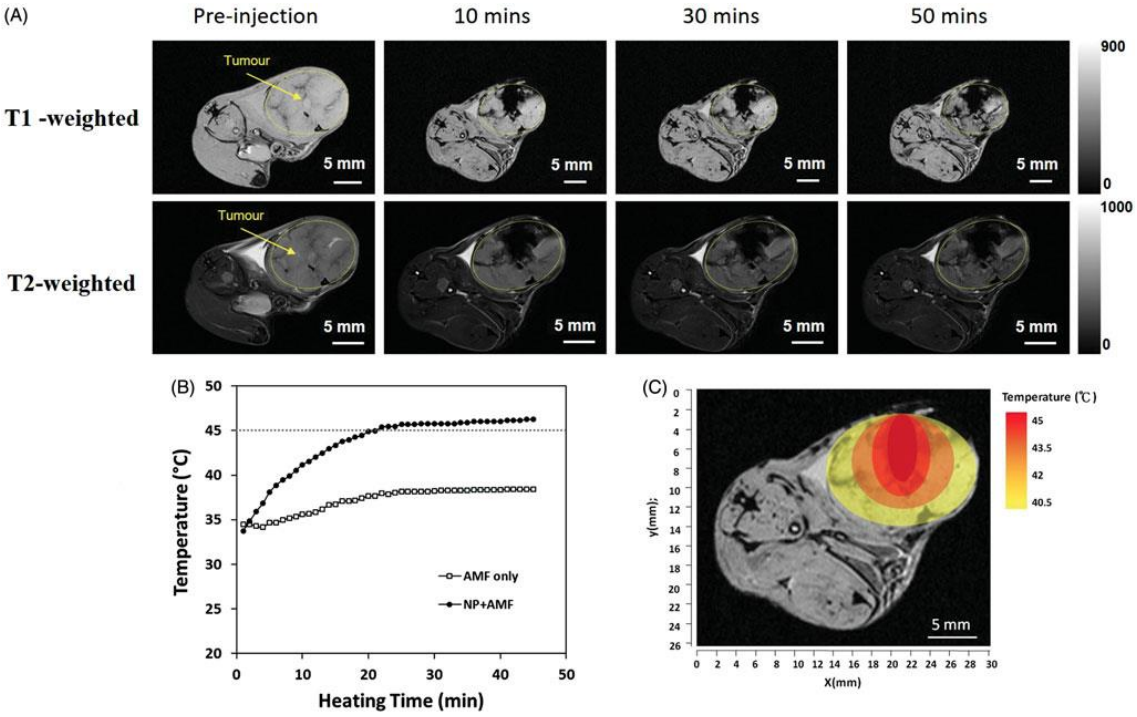

Fig. 2 (A) The retention of GdIONPs in the TRAMP-C1 tumor shown by T1 and T2-weighted MR imaging taken at different times. The injected GdIONPs were remained in the TRAMP-C1 tumors (highlighted by the yellow outline) for 10, 30, and 50 mins. (B) The temperature distribution profile changes across heating time measured by a thermocouple needle at the GdIONP injection site. The thermotherapy was conducted by an induction heating at an external alternating magnetic field (AMF, 52 kHz and 246 Oe) for 40 mins. Mice were injected with PBS (AMF only) or GdIONP (AMF+NP) under external alternating magnetic field (AMF). (C) The simulated temperature distribution within tumor. The tumor temperature decreased by 1.5-degree Celsius for every 2 mm away from the TT core.

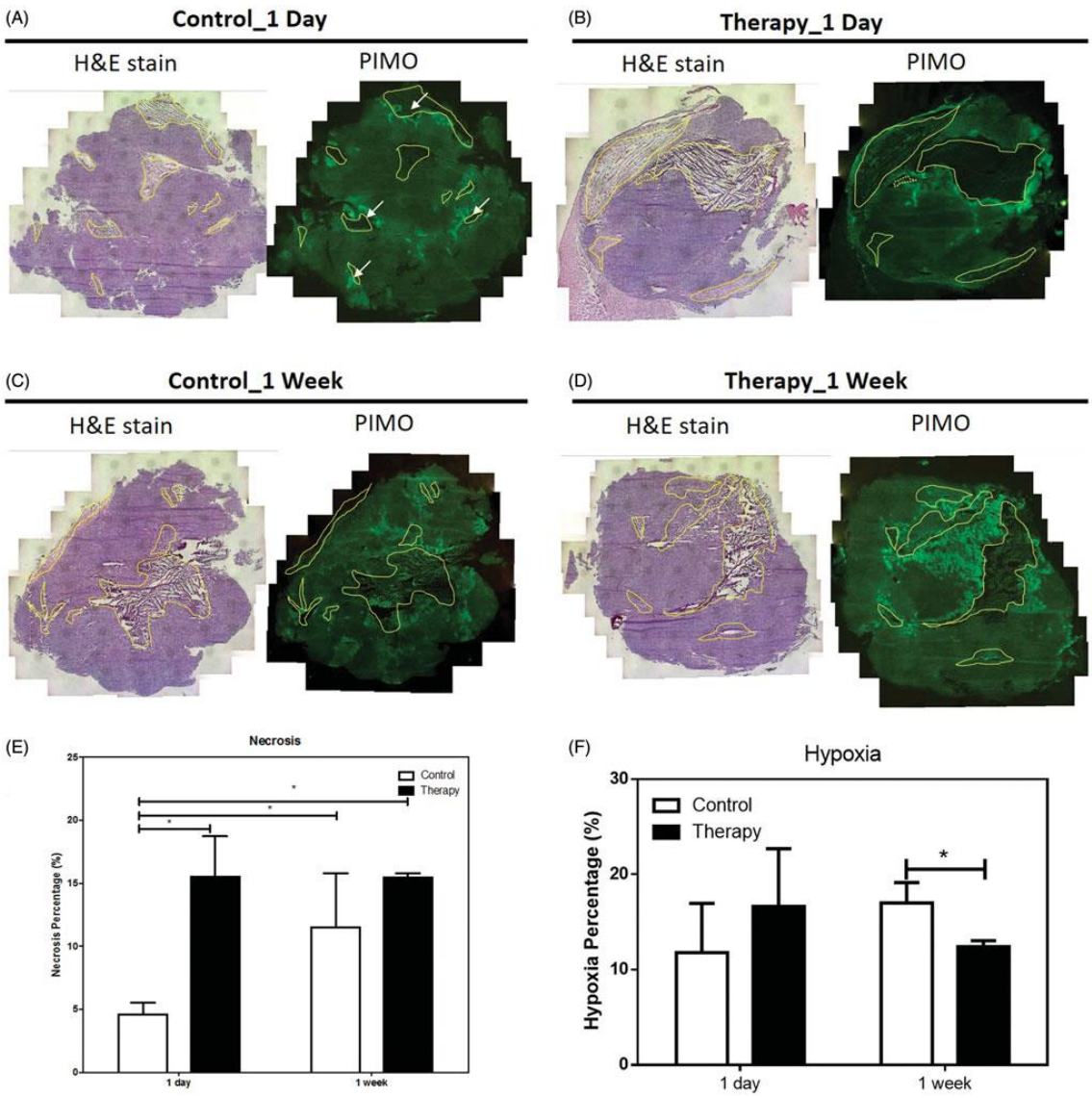

Fig. 3 H & E and PIMO staining of tumor of control (A and C) and thermotherapy (B and D) 1 day (A and B) and 1 week (C and D) after treatment. The percentage of necrosis (E) and hypoxia (F) of the control and thermotherapy (TT)-treated TRAMP-C1 tumors at day one and week one after TT. The largest cross section of the TRAMP-C1 tumor was used to normalize the necrosis and hypoxia areas. Necrosis region were delineated by the yellow outlines. The pimonidazole (PIMO) was administrated i.v. injection for detecting hypoxia. Bars indicate the SE of 3 to 5 tumors at each time point. The hypoxia fraction was defined as the area positive of pimonidazole divided by the total tumor area (necrosis excluded). *: P <0.05.

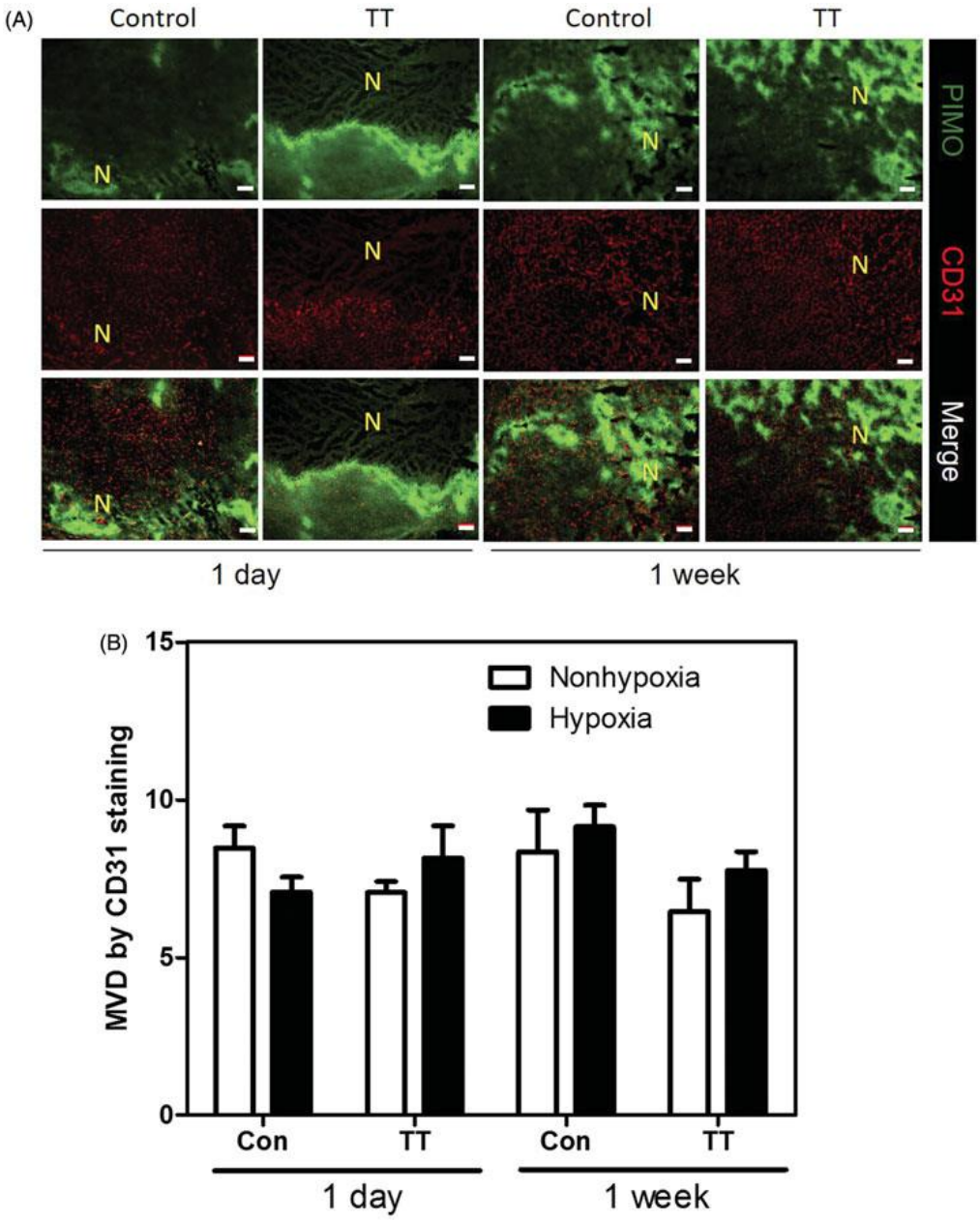

Fig. 4 (A) The distribution of necrosis denoted by N, hypoxia stained by PIMO (green colour), and vasculature stained by CD31 (red colour) in control and TT treated TRAMP-C1 tumors at 1 day and 1 week after treatment. The scale Bar equals 100 μm (B) The change of MVD in hypoxic and nonhypoxic regions of the control and TT-treated TRAMP-C1 tumors at day one and week one after TT is shown as a bar graph. MVD was defined by the percentage of CD31+ area to the total tumor in field of view. The Bars indicate the SE of measurements from 5 fields (non-necrotic areas) of 3 to 5 tumors for each time point.

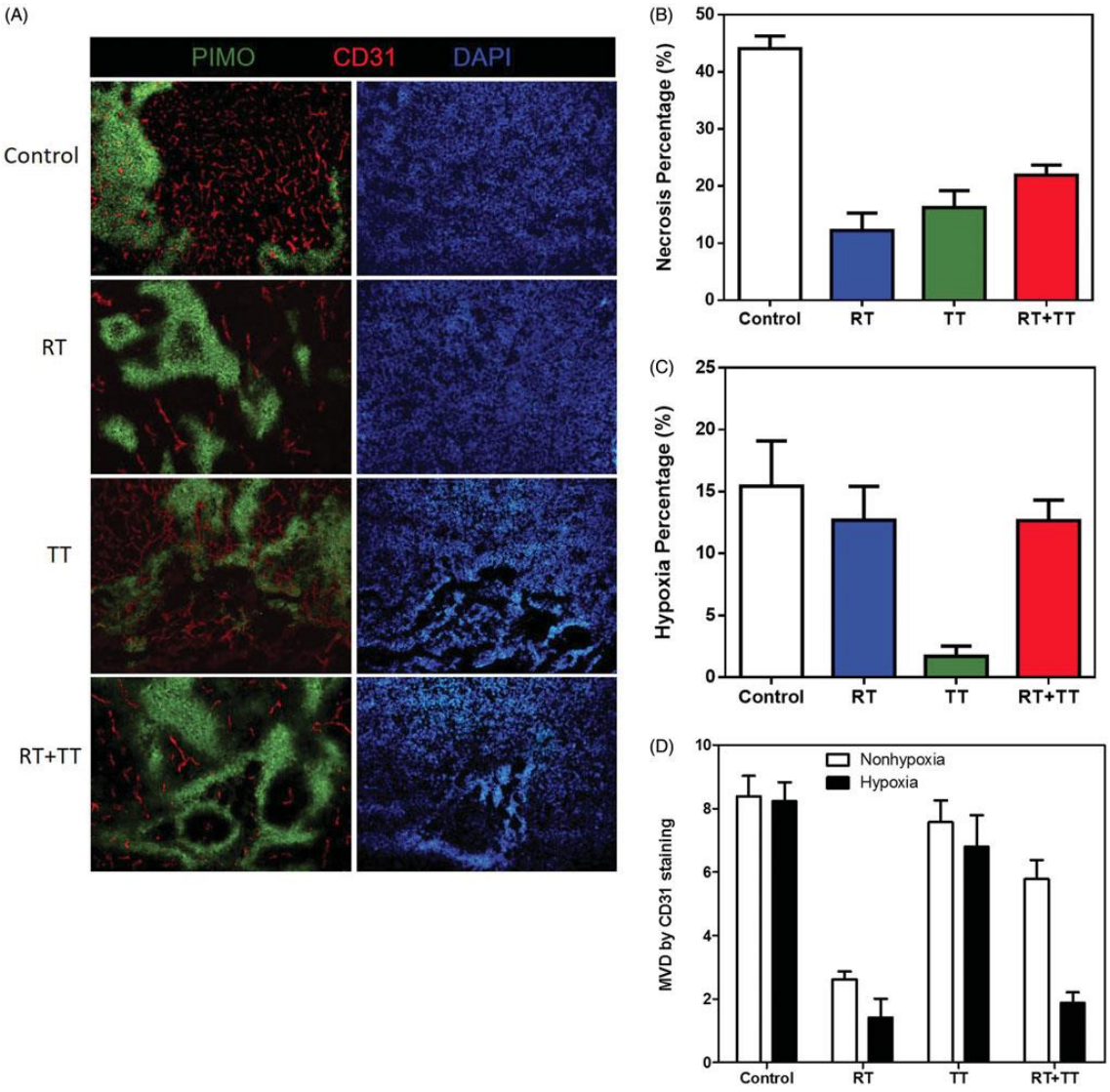

Fig. 5 (A) hypoxia (green), vasculature (red), and nuclei (blue) areas revealed by immunofluorescence staining for the control (10 days), RT (15 days), TT (15 days), and combined therapy (15 days) treated TRAMP-C1 tumors. The change of (B) necrosis, (C) hypoxia, and (D) MVD in hypoxic and nonhypoxic regions of control and TT-treated tumors were represented using a bar graph. There was almost no vasculature in the hypoxia regions of irradiated tumors (RT and combined therapy). Bar: SE of 5 fields (non-necrotic areas) of 3 to 5 tumors for each time point.

Supplementary material

Gadolinium-doped iron oxide nanoparticles (GdIONP) synthesis

The Gd-doped iron oxide nanoparticles (GdIONP) were synthesized under an argon atmosphere. The standard procedure is outlined below. A reaction flask was charged with $FeCl_2$ (0.0345 moles), $FeCl_3$ (0.069 moles) and deionized water (150 ml). To produce the Gd-doped sample $FeCl_3$ was replaced by the appropriate amount of GdCl3. NaOH with a concentration of 5 M was added to control the pH value of the mixture. The mixture was subjected to continuous stirring during the reaction until the mixture became basic (the pH value approached 11.5). The temperature of the mixture was then raised to 65 °C for 10 min. The black precipitate formed was washed with deionized water and the pH adjusted to below 5 with glacial acetic acid. Finally, H_2O_2 (10 vol %) was gradually added until no further reaction occurred. This was judged as the point at which no further effervescence occurred on addition of fresh H_2O_2 followed by a deionized water wash. Note that before the precipitates were formed all procedures were performed under argon.

The nanoparticle synthesis produced very stable dispersions with no obvious precipitation after several days. The appearance of the GdIONP was identical to the standard IONP. The magnetic properties were determined with a vibrating sample magnetometer (VSM). From the magnetisation curve shown in Fig. S1 it can be seen that the GdIONPs are superparamagnetic with a magnetisation value (Ms) of 65.67 emu g^{-1}. Elemental analysis by ICP-AES confirmed the presence of the Gd and gave atomic ratios of 0.007: 1 (Gd : Fe). From this it can be estimated that 25% of the Gd^{3+} present in the reaction mixture was incorporated into the final particles giving a particle composition of $Gd_{0.02}Fe_{2.98}O_4$. The X-ray diffraction (XRD) spectrum can be seen in Fig. S2. This shows that the GdIONP retains the magnetite lattice structure of Fe_3O_4. The reflection from the 311 lattice face can be used to estimate the average crystallite size by applying the Scherrer model, this can be written as $d = 0.9\lambda/\beta\cos\theta$, where • = 0.154 nm for the CuKa line, d is the crystallite diameter β is the full width at half maximum of the 311 peak in radians and h is the peak position. Applying this formula to the spectrum shown in Fig. S2 gives an average crystallite size of 13 nm. The TEM image of the nanoparticles can be seen in Fig. S3. This shows the particles have distinct lattice faces characterised by cubic or rhombus features with a high degree of crystallinity. The average particle size calculated from image analysis is 13.2 ± 3.1 nm, this is in good agreement with the average crystallite size estimated from the XRD data.

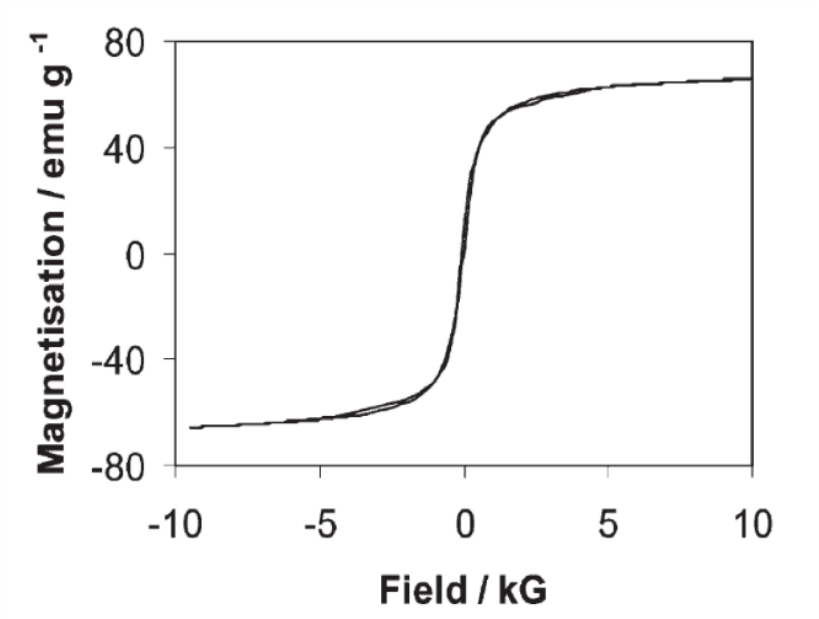

Fig. S1: magnetisation curve for the GdIONPs

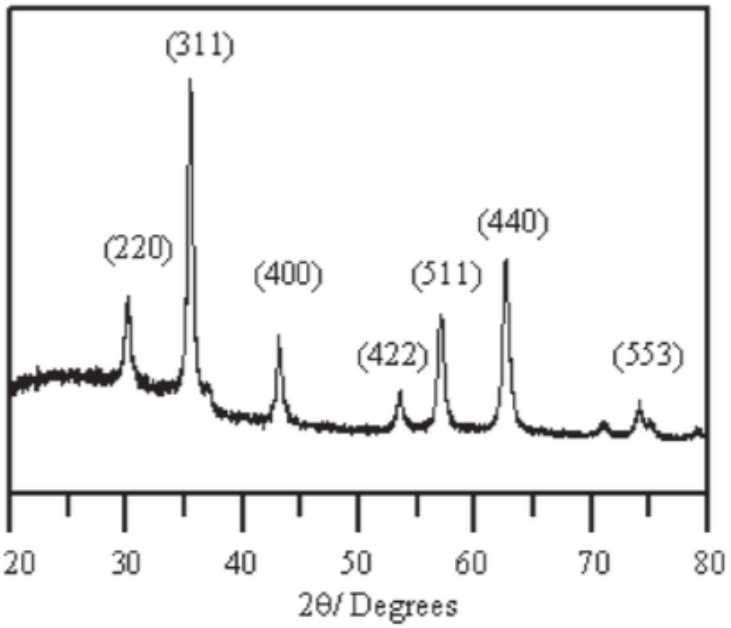

Fig. S2: X-ray diffraction spectrum for the GdIONPs

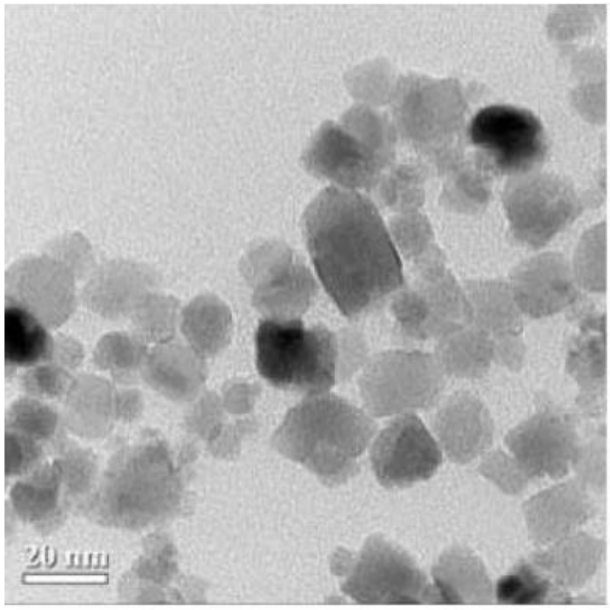

Fig. S3: TEM image of the GdIONPs

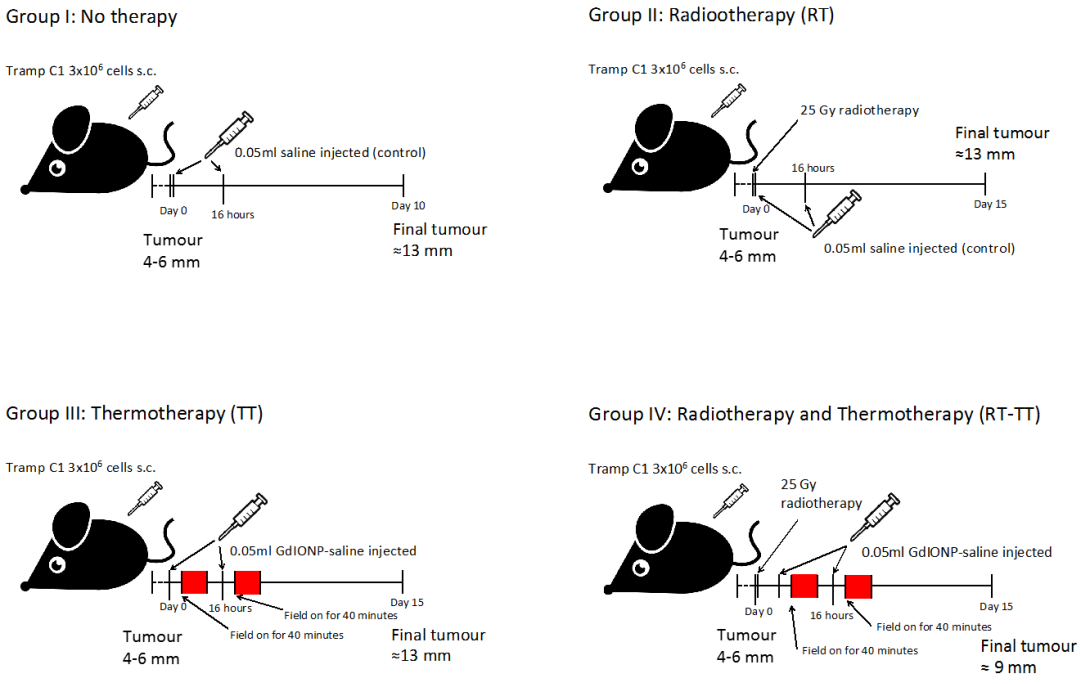

Fig. S4: schematic representation of the injection and therapy protocols. For mice receiving two injections of either nanoparticles or saline solutions for the blank control group, the 1st injection were conducted at the start of treatment or after RT, and the 2nd injection were carried out 16 hours after the 1st injection.